

Fully Rollable Lead-Free Poly(vinylidene fluoride)-Niobate-Based Nanogenerator with Ultra-Flexible Nano-Network Electrodes

Chen Zhang,^{†,‡} Youjun Fan,^{‡,||} Huayang Li,^{‡,||} Yayuan Li,[†] Lei Zhang,^{‡,∇} Shubo Cao,[†] Shuangyang Kuang,^{‡,||} Yongbin Zhao,[●] Aihua Chen,^{*,†,⊥} Guang Zhu,^{*,‡,§,||} and Zhong Lin Wang^{*,‡,||,♯}

[†]School of Materials Science and Engineering, Beihang University, Beijing 100191, China

[‡]CAS Center for Excellence in Nanoscience, Beijing Key Laboratory of Micro-nano Energy and Sensor, Beijing Institute of Nanoenergy and Nanosystems, Chinese Academy of Sciences, Beijing 100083, China

[§]Department of Mechanical, Materials and Manufacturing Engineering, The University of Nottingham Ningbo China, Ningbo 315100, China

[⊥]Beijing Advanced Innovation Centre for Biomedical Engineering, Beihang University, Beijing 100191, China

^{||}School of Nanoscience and Technology, University of Chinese Academy of Sciences, Beijing 100048, China

[♯]School of Materials Science and Engineering, Georgia Institute of Technology, Atlanta, Georgia 30332, United States

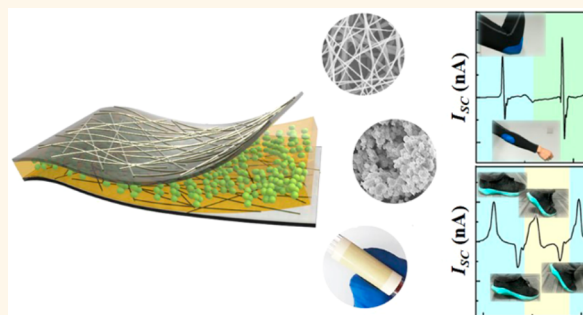
[∇]Key Laboratory of Advanced Technologies of Materials (Ministry of Education), School of Materials Science and Engineering, Southwest Jiaotong University, Chengdu 610031, China

[●]Shandong Oubo New Material Co. Ltd, Dongying, Shandong 257088, China

Supporting Information

ABSTRACT: A fully rollable nanocomposite-based nanogenerator (NCG) is developed by integrating a lead-free piezoelectric hybrid layer with a type of nanofiber-supported silver nanowire (AgNW) network as electrodes. The thin-film nanocomposite is composed of electroactive polyvinylidene fluoride (PVDF) polymer matrix and compositionally modified potassium sodium niobate-based nanoparticles (NPs) with a high piezoelectric coefficient (d_{33}) of 53 pm/V, which is revealed by the piezoresponse force microscopy measurements. Under periodical agitation at a compressive force of 50 N and 1 Hz, the NCG can steadily render high electric output up to an open-circuit voltage of 18 V and a short-circuit current of 2.6 μ A. Of particular importance is the decent rollability of the NCG, as indicated by the negligible decay in the electric output after it being repeatedly rolled around a gel pen for 200 cycles. Besides, the biocompatible NCG can potentially be used to scavenge biomechanical energy from low-frequency human motions, as demonstrated by the scenarios of walking and elbow joint movement. These results rationally expand the feasibility of the developed NCG toward applications in lightweight, diminutive, and multifunctional rollable or wearable electronic devices.

KEYWORDS: fully rollable, nanocomposite-based nanogenerator, niobate-based nanoparticles, silver nanowire-based electrodes, wearable electronic devices



With the rapid growth of portable electronics, wearable devices, and wireless sensing networks, considerable efforts have been devoted to the development of abundant, sustainable, and environmentally benign energy sources.¹ Over the past decade, flexible piezoelectric nanogenerators (PENGs) have been extensively investigated not only for self-powered electronic systems but also as active sensors for real-time monitoring,^{2–5} by virtue of

that it can effectively harvest diverse types of mechanical energy from deformations,⁶ vibrations,^{7,8} fluid/air flows,^{9,10} acoustic waves,^{11–13} and even body/organ motions.^{14,15} To date, various nanostructures have been proposed for PENGs based

Received: February 27, 2018

Accepted: April 27, 2018

Published: April 27, 2018

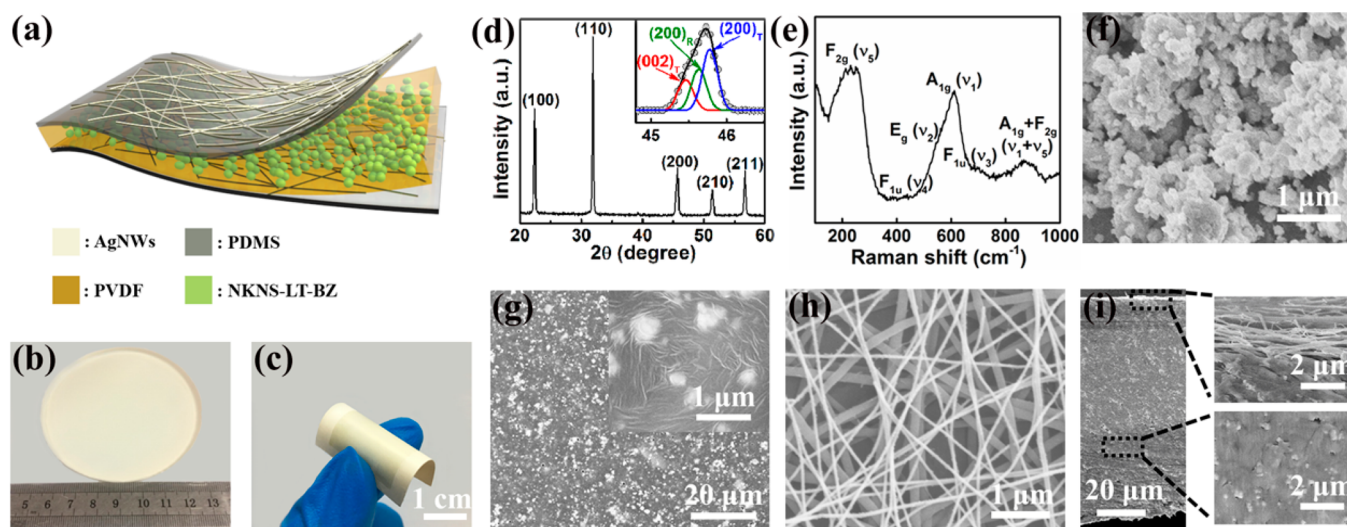


Figure 1. (a) Schematic illustration presenting the structure of the PVDF-niobate-based NCG with the AgNW-based electrodes. (b,c) Optical photographs of an as-fabricated wafer-scale nanocomposite thin film (7.5 cm in diameter) and an integrated NCG at bent state that exhibits its bending flexibility. (d–f) XRD pattern, Raman spectrum, and SEM image of the uniform-sized NKNS-LT-BZ NPs synthesized by a solid-state reaction, showing a perovskite crystalline structure with the coexistence of ferroelectric rhombohedral and tetragonal phases. (g) Top-view SEM image of the annealed thin-film nanocomposite with well dispersed NKNS-LT-BZ NPs. The inset shows a locally magnified region, indicating the needle-like morphology of the PVDF matrix. (h) Top-view SEM image of the nylon nanofiber-supported AgNW-based electrode. (i) Cross-sectional SEM image of the PVDF-niobate-based NCG.

on ZnO nanowires,^{16,17} GaN nanorods,¹⁸ MoS₂ nanoflakes,¹⁹ conventional piezoceramic crystals,^{7,20–23} organic–inorganic lead halide perovskites,²⁴ and polyvinylidene fluoride (PVDF).^{8–10} In particular, the nanocomposite-based nanogenerator (NCG) composed of elastic matrix and nanoscaled piezoelectric fillers has emerged as a new paradigm with improved mechanical flexibilities and enhanced output performances.^{14,15,25–31} Moreover, such merits as simple structure, low cost, and easy fabrication are likewise advantageous for possibly large-scale energy harvesting.^{14,26,27} Even so, several deficiencies, including poor mechanical strength and still low-level electric output, are bound to be addressed in order to meet the ever-increasing demands of the practical applications.³²

β -Phase PVDF and its copolymers are among the most attractive organic piezoelectric materials because of their superior piezoelectric properties, adequate mechanical robustness, and desirable flexibility.⁵ Despite a variety of PVDF-based architectures having been designed for PENGs,^{8–10,33} it still has rarely been employed as the matrix of the NCG. Only recently, Shin et al. developed a composite thin film composed of BaTiO₃ (BT) nanoparticles (NPs)-poly(vinylidene fluoride-*co*-hexafluoropropene) (P(VDF-HFP)) hemispherical clusters, which exhibited surprisingly high piezoelectric power output owing to dipoles centralization combined with effective stress transfer.³⁴ More recently, Siddiqui et al. also reported a well performed poly(vinylidene fluoride-*co*-trifluoroethylene) (P(VDF-TrFE))-based NCG by introducing BT NPs as well.³⁵ Considering that the voltage generated by the NCG primarily depends on the piezoelectric coefficient (d_{33}) of the inorganic component, special attention should thus be paid to materials with excellent piezoelectric activity.³¹ In this regard, (Na,K)-NbO₃ (NKN), as a kind of biocompatible lead-free piezoelectric material, has been widely studied because its piezoelectric property can be significantly promoted by simple compositional modification.³⁶ The usual way to achieve this is to form the polymorphic phase boundary (PPB) at room

temperature by either adding dopants, such as Li⁺, Ta⁵⁺, and Sb⁵⁺, or by forming solid solutions with compounds, including (Bi_{0.5}Na_{0.5})TiO₃, NTiO₃ (N: Ba²⁺, Ca²⁺, Mg²⁺, and Sr²⁺), and BiMO₃ (M: Fe³⁺, Sc³⁺, and Al³⁺).³⁷ The reduced energy barrier for polarization rotation within the PPB compositions of the NKN-based systems could conduce to outstanding piezoelectric activities ($d_{33} > 300$ pC/N) compared to BT ($d_{33} \sim 100$ pC/N), closely matching to those of toxic Pb-based piezoceramics, which make them more suitable for NCG.²⁷

Moreover, although a number of bendable NCGs have been frequently studied, the authentically operating rollable NCG has been still scantily developed due to the absence of proper electrodes and robust nanocomposite matrix.^{24–31} Herein, we develop a simple and facile route to a fully rollable lead-free PVDF-niobate-based NCG with high performance, in which a compositionally modified NKN-based piezoelectric material with nominal composition of 0.915(Na_{0.5}K_{0.5})(Nb_{0.94}Sb_{0.06})O₃-0.045LiTaO₃-0.04BaZrO₃ (NKNS-LT-BZ) is adopted (see Note S1 for details). This composition is found to be located in the PPB region with the coexistence of rhombohedral and tetragonal phases, giving rise to exceptional piezoelectric properties for the NPs ($d_{33} \sim 53$ pm/V). The thin-film nanocomposite made of well distributed NKNS-LT-BZ NPs and PVDF polymer matrix is fabricated via a solution casting process in wafer scale. A type of ultraflexible nanofiber-supported silver nanowire (AgNW) network is adopted as the electrode, which is integrated with the nanocomposite so as to realize rollability for the NCG. Under periodical agitation at a compressive force of 50 N and 1 Hz, the NCG with an area size of 2 × 2 cm² can generate an open-circuit voltage (V_{OC}) of 18 V and a short-circuit current (I_{SC}) of 2.6 μ A. The optimal content of the NKNS-LT-BZ NPs is found to be 30%. In particular, the electric outputs have negligible reduction after being rolled around a gel pen for 200 cycles, which reveals decent rollability of the NCG and presents their applicability for tubular devices. Besides, the demonstrations of the NCG in harvesting biomechanical energy from low-frequency human

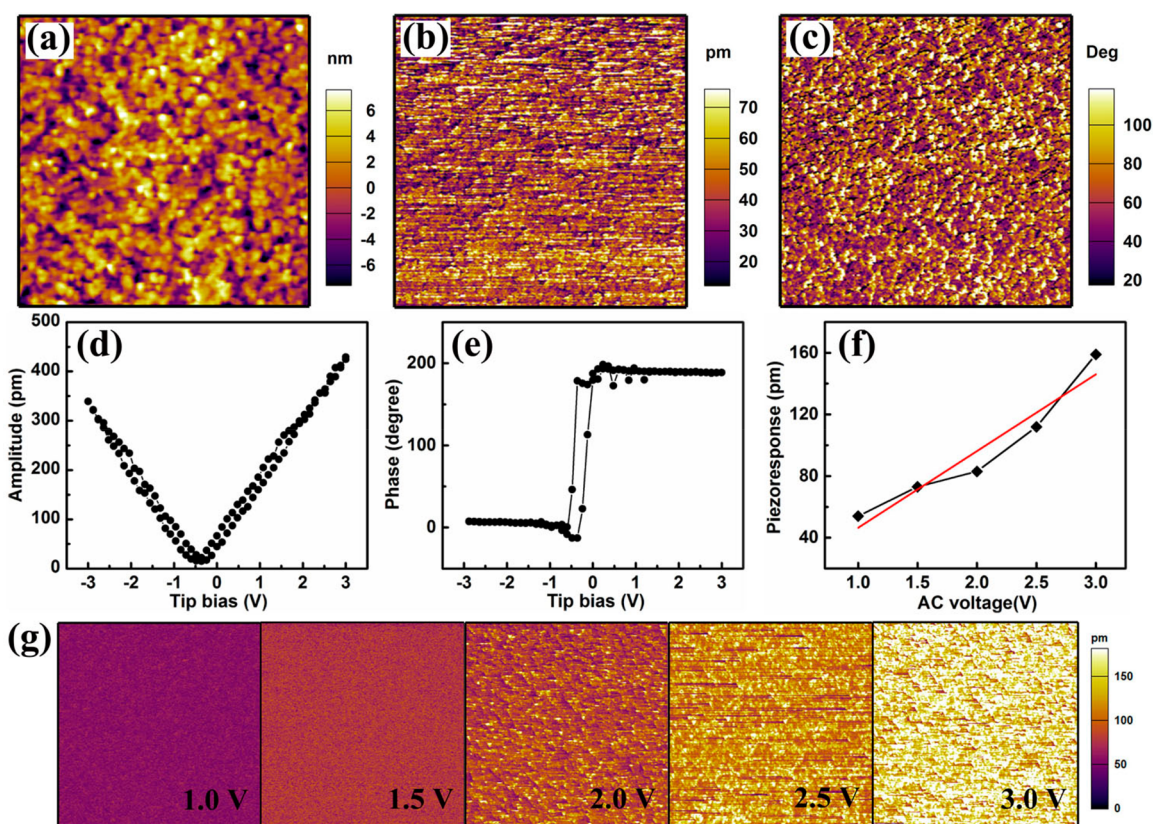


Figure 2. (a–c) Topography, amplitude, and phase images of the NKNS-LT-BZ NPs, respectively. Local OP-PFM (d) amplitude and (e) phase hysteresis loops obtained by applying a DC voltage of 3 V. (f) The AC-voltage dependent piezoresponse and the corresponding (g) amplitude images measured from different AC-voltages. All the images are scanned within an area of $5 \times 5 \mu\text{m}^2$.

body motions, such as walking and elbow bending, indicate that they can be possibly used in lightweight, diminutive, and multifunctional wearable electronic devices.

RESULTS AND DISCUSSION

A schematic structure of the flexible PVDF-niobate-based NCG is illustrated in Figure 1a. The piezoelectric nanocomposite layer comprised of well-embedded NKNS-LT-BZ NPs and PVDF polymer matrix with a diameter of 7.5 cm is first fabricated through a solution casting method (Figure 1b). Subsequently, a type of ultrathin, highly conductive, and super flexible nylon nanofiber-supported AgNW-based electrode is seamlessly assembled on both sides of the nanocomposite with the assistance of an adhesive layer of polydimethylsiloxane (PDMS). The sheet resistance of the AgNW-based electrode is obtained to be as low as $8.6 \Omega \text{sq}^{-1}$ and barely changes in spite of repeated bending, which exhibits its superior mechanical robustness and flexibility as compared to commercial ITO electrode (Figure S1).^{38–40} Here, a photograph that demonstrates the bending flexibility of the fabricated NCG is displayed in Figure 1c.

The compositionally modified NKNS-LT-BZ NPs adopted here were synthesized via a conventional solid-state reaction method (see the Experimental Section). X-ray diffraction (XRD) and Raman spectroscopy were carried out to characterize the crystalline structure of the NPs. All XRD diffraction peaks are precisely distinguishable and can be indexed to the lattice planes of the perovskite structure (Figure 1d). Notably, the magnified asymmetric (200) diffraction peak, which is the characteristic one of tetragonal symmetry, is fitted by a pseudo-

Voigt function as shown in the inset of Figure 1d. The resultant $(002)_T/(200)_T$ and $(200)_R$ peaks indicate that the composition of the NKNS-LT-BZ NPs lies in the PPB region with the coexistence of rhombohedral and tetragonal phases. Moreover, the Raman spectrum of the NPs are in great consistency with general NKN-based perovskite materials (Figure 1e).²⁷ Because of the random growth orientation of the NPs, the profiles of vibration modes are relatively broad compared with those of a single crystal.⁴¹ The intermediate and high-frequency vibrations are associated with NbO_6 octahedra, consisting of $A_{1g}(\nu_1)$, $E_g(\nu_2)$, $F_{1u}(\nu_3)$, $F_{1u}(\nu_4)$, and $F_{2g}(\nu_5)$ in the range of $200\text{--}900 \text{cm}^{-1}$.⁴² Particularly, several subtle signs, such as the weak $E_g(\nu_2)$ shoulder at 550cm^{-1} and the small $F_{1u}(\nu_4)$ mound in the region from 360 to 460cm^{-1} , also suggest the coexistence of ferroelectric phases in the NPs.⁴³ Figure 1f presents a scanning electron microscopy (SEM) image of the NKNS-LT-BZ NPs in polydisperse angulated shape with the feature size from 50 to 300nm . After sufficient stirring and ultrasonic dispersing, the NPs can be uniformly distributed in the PVDF polymer matrix (Figure 1g). Meanwhile, the typical needle-like morphology of the ferroelectric β -phase PVDF is observed in a magnified SEM image, shown in the inset of Figure 1g. This phenomenon agrees well with the Fourier transform infrared spectroscopy (FT-IR) results obtained from the conventional PVDF films (Figure S2). The presence of nonpolar α -phase in the pristine PVDF film is found to be evident with a set of strong vibrational bands at 533 , 613 , 762 , 795 , 856 , 974 , 1148 , and 1208cm^{-1} . In contrast, three new bands at 510 , 840 , and 1285cm^{-1} , in an annealed PVDF film, belong to CF_2 stretching with the dipole moments parallel to the polar b -axis, which confirms

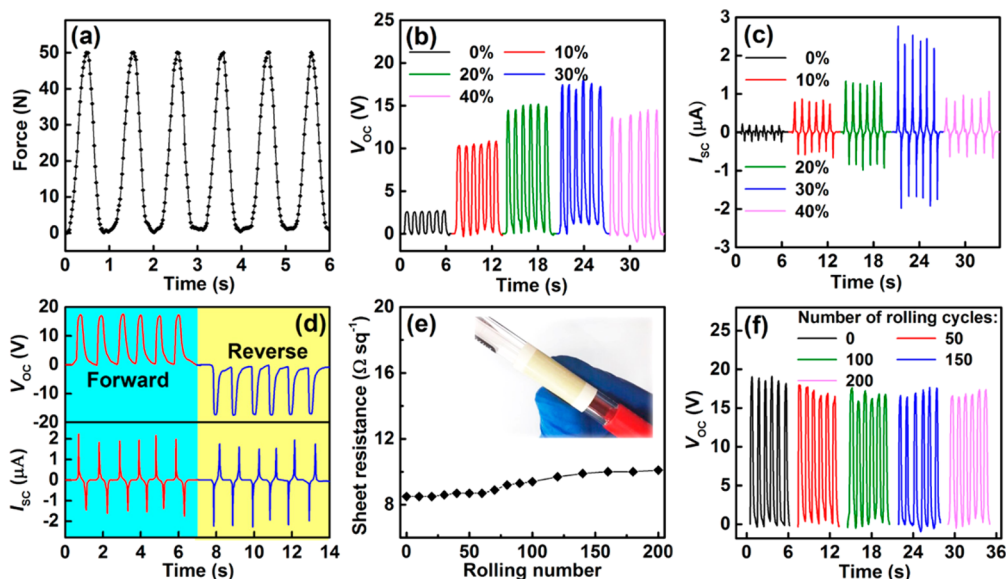


Figure 3. Electric characterization of the PVDF-niobate-based NCGs. (a) Cycled compressive force vertically loaded onto the NCGs, and the corresponding cycled (b) V_{OC} and (c) I_{SC} of the NCGs with different NKNS-LT-BZ NPs content from 0 to 40%. (d) Results of the polarity-switching test (forward and reverse connections) conducted to demonstrate the measured electric output indeed stem from the NCG rather than the instruments. (e) Sheet resistance of the AgNW-based electrode integrated on the NCG as a function of the rolling number. The inset shows an optical photograph presenting a NCG fully rolled on a gel pen with a diameter of 8 mm. (f) The corresponding V_{OC} does not decay after rolling, indicating the decent rollability of the NCG.

the formation of electroactive β -phase.^{44,45} Figure 1h shows a top-down SEM image of the nylon nanofiber-supported AgNW network. It can be observed that the AgNWs with an average diameter of 25 nm and a length of 5–20 μm are uniformly distributed into a layer of nylon nanofibers of about 100 nm in diameter. The AgNWs and the nylon nanofibers are intertwined, which enables the nanonetwork electrode to possess high conductivity, flexibility, and mechanical robustness. Cross-sectional SEM images of the fabricated NCG are shown in Figure 1i. The thickness of the thin-film nanocomposite can be facilely controlled to around 80 μm by the amount of casting slurries. From the enlarged view, good dispersity of the NKNS-LT-BZ NPs can be also observed, which is beneficial to effective stress transfer and further to piezopotential generation.^{27,35}

In order to investigate the local polarization state as well as the dynamic domain switching behavior of the NKNS-LT-BZ NPs, piezoresponse force microscopy (PFM) measurements were conducted. Figure 2a–c shows the topography, the out-of-plane (OP) amplitude, and phase images of the NPs with a scanned area of $5 \times 5 \mu\text{m}^2$, respectively. The images were recorded in a dual AC resonance tracking (DART) mode using an AC driving voltage of 2 V at a deflection setting point of 0.5 V and a scanning frequency of 1 Hz. The topography in Figure 2a shows the dense and homogeneous NPs with an average grain size of 150 nm, which is in conformity with the SEM observation (Figure 1f). Domains with opposite polarization orientation can be identified by the image contrast in Figure 2c. The dark brown and bright yellow regions correspond to domain polarization that is oriented upward and downward, respectively. Moreover, the typical butterfly shaped amplitude loop and rectangular-shaped phase hysteresis loop were measured by applying a sequence of DC bias voltage along the tip axis to explore the local piezoresponse and ferroelectricity of the NPs. As presented in Figure 2d, the asymmetry of the amplitude loop is likely due to the built-in

piezoelectric field and the domain movement under the tip region. In the measurement configuration, a highly nonuniform electric field could develop under the tip, which would produce a certain in-plane driving force to move or bend the non-180° domains.⁴⁶ The slim phase angle loop (Figure 2e) shows a 180° difference. This result proves that the dipoles are easily capable of being switched by an external electric field, which is also clearly indicated by the *in situ* poling process (Figure S3). The shift toward negative bias in the loop can be ascribed to the polarization pinning owing to either charge trapping or mechanical stress.^{46,47} In addition, both the strong piezoresponse and the low coercive field derived from the amplitude and phase angle loops, respectively, are benefited from the coexistence of the ferroelectric phases in the NPs. Since the magnitude of the d_{33} coefficient is proportional to the electromechanical response of a material, the d_{33} of the NKNS-LT-BZ NPs can be calculated by measuring the AC voltage-dependent amplitude image,³¹ as shown in Figure 2f,g. The effective d_{33} value of the NPs is about 53 pm/V, which is superior to that of NaNbO₃ nanowires (4 pm/V), (Bi_{0.5}Na_{0.5})-TiO₃ nanofibers (18 pm/V), and even FAPbBr₃ (25 pm/V) or BT (28 pm/V) NPs.^{31,48} These results exhibit fairly good piezoelectric and ferroelectric properties of the NKNS-LT-BZ NPs, making them well suitable for mechanical energy harvesting.

The electric output of the NCGs in this work is evaluated by applying a repeated compressive force from an impact stimulator (see Note S2 for details). All of the NCGs are pretreated with poling process to align the randomly oriented dipoles in the domains. Under the force of 50 N at a frequency of 1 Hz (Figure 3a), the open-circuit voltage (V_{OC}) and short-circuit current (I_{SC}) were recorded from the NCGs with different NKNS-LT-BZ NPs content. As shown in Figure 3b,c, a V_{OC} amplitude of 2.5 V and a I_{SC} of 0.2 μA are obtained for the NCG without the NPs as a control group. As previously reported, the electric output from PVDF-based PENGs was

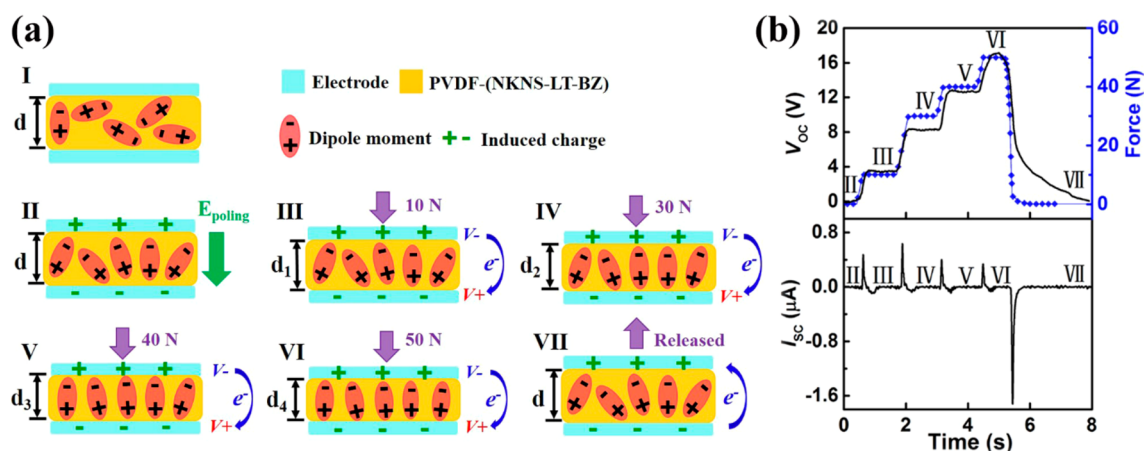


Figure 4. (a) Schematic illustration clarifying the energy conversion mechanism of the PVDF-niobate-based NCG. The generation and vanishment of the piezopotential drive the electron flow forward and backward, respectively. (b) The electric output of V_{OC} and I_{SC} varies with the different vertical mechanical force.

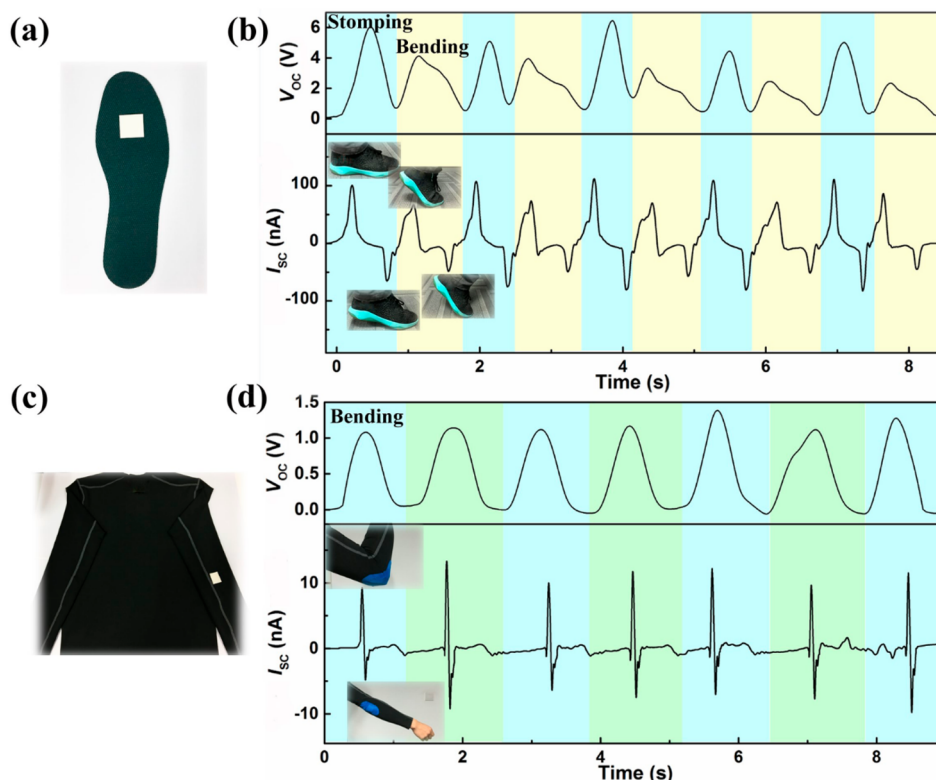


Figure 5. Demonstration of the PVDF-niobate-based NCG potentially harvesting biomechanical energy from low-frequency human motions. (a) Optical photograph of a NCG with a size of $3 \times 3 \text{ cm}^2$ glued onto a shoe-pad. (b) Experimentally measured V_{OC} and I_{SC} from the NCG during human walking. Two types of electric output are observed corresponding to the two different motions, i.e., stomping and walking-enabled bending. (c) Optical photograph of a NCG with a size of $3 \times 3 \text{ cm}^2$ taped to the elbow of a tight sport suit and seamlessly stitched by a piece of cloth. (d) Generated V_{OC} and I_{SC} from the NCG by bending and straightening an arm.

usually small, which is largely due to the weak dipole polarization of the PVDF.^{49–51} With the increase of the NKNS-LT-BZ NPs content, both V_{OC} and I_{SC} present a steady increase until the NPs content reaches 30%. The maximum electric output of 18 V and $2.6 \mu\text{A}$ is achieved. This substantial enhancement of the electric output is attributed to the reinforced piezoelectricity of the nanocomposite, which resulted from the well-known interfacial or Maxwell–Wagner–Sillars polarization occurring at the interfaces between the NPs and PVDF matrix. However, as the NPs content

further increases, the emerging massive aggregations (Figure S4d) tend to unduly narrow the distance among the NPs accompanied by the solidification of dipole moments. Although the dielectric constant and polarizability could rapidly increase in this case, the electric breakdown might take place due to the more and more weak insulation of the nanocomposite.⁵² As a result, the electric output no longer increases but drops down to 14 V and $1 \mu\text{A}$ when the NPs content reaches up to 40%. This observation is consistent with previous reports on PVDF-based NCGs,^{34,35} indicating that compositional optimization is

essential for high-performance NCGs. To confirm that the electric output genuinely originates from the NCGs rather than the measurement system, a polarity-switching test was carried out. Both V_{OC} and I_{SC} in forward and reverse connections exhibit opposite polarity with almost identical amplitude, as revealed in Figure 3d, which attests the genuineness of the electric output.

In addition, the adequate flexibility and rollability of the NCG are further investigated. The inset in Figure 3e illustrates a fully rolled NCG wrapping around a gel pen with a diameter of 8 mm. All the same, the AgNWs are uniformly distributed into the layer of nylon nanofibers without visible crimp, twist, and snap after the rolling (Figure S5). As a result, although the sheet resistance of the AgNW-based electrode slightly increases with respect to the number of rolling cycles, it still can be maintained at a low value about $10 \Omega \text{ sq}^{-1}$ after being rolled for 200 cycles. Accordingly, decay in the V_{OC} output for the NCG is not observed after the rolling, as shown in Figure 3f. The decent rollability of the NCG indicates its possible applications, such as fully rollable portable devices,⁵³ tubular motion sensors,⁵⁴ and energy-harvesting systems in automobile tires.¹⁵

Figure 4a,b illustrates the energy conversion mechanism of the PVDF-niobate-based NCG as being stressed. At the original state, each piezoelectric domain that contains electric dipoles in the nanocomposite is randomly oriented, exhibiting absolute nonpolarity (Figure 4a, I). During the following poling process, the polarization orientation of each domain would tend to align along the electric field direction through the domain wall motions. Some domains will be oriented parallel to the electric field direction, yet some just tilt after the removal of the external bias, resulting in a strong remanent polarization. Therefore, both the top and bottom electrode surface would possibly trap a certain amount of bound charges with opposite sign to screen the built-in piezoelectric field (Figure 4a, II). In this state, there is no piezopotential coming forth because of the zero net electric dipoles. However, while a vertical compressive stress is applied to the NCG, the dipoles inside the domains would align in a single direction more strongly due to the stress-induced poling effect, which is believed to be reinforced with increasing the applied stress.³¹ As a result, the piezopotential is immediately generated across the top and bottom electrodes (Figure 4a, III–VI). Accordingly, the step-like V_{OC} output presented in Figure 4b is found to be in a close correspondence with the applied force. This means that the amplitude of the generated piezopotential could remain constant under a given stress, which in turn certifies the genuineness of the stress-induced piezopotential and also makes the NCG promising for pressure sensor applications. Besides, in the case of short-circuit condition, the electron flow will be driven to counteract the piezopotential change along the stress direction, illustrated by the set of transient current pulses (Figure 4b). Once the external compressive stress is released, the piezopotential will be vanished, and the electrons accumulated on the bottom electrode will instantly transit back to the opposite direction (Figure 4a, VII). Therefore, pulse-type voltage and AC-type current electric output can be produced under repeated vertical compression and release (Figure 3b,c).

Since the developed NCG is able to generate considerable electric output in response to mechanical pressing at a low frequency, it can be potentially used to scavenge biomechanical energy from human body motions. As demonstrated in Figure 5a, a NCG is taped onto a shoe-pad to harvest energy from

human walking. Two types of electric output were obtained in accordance to the two different motions, i.e., stomping and walking-enabled bending, as illustrated by the snapshots in Figure 5b. The stomping motion can produce a relatively high electric output of approximately 6 V and 100 nA, whereas the bending stimuli yield a lower electric output of 4 V and 70 nA. This result is attributed to the more powerful and faster interaction during the stomping stage. With sequential repeat of these two processes, the NCG is pressed and bent in a cyclic manner, respectively. Thus, it can sustainably generate electric energy during walking, which is fully comparable to that of the previously reported elastic-composite nanogenerators.^{15,55} The harvested electric energy can be directly stored in electrolytic capacitors through a full wave bridge rectifier circuit and used to power green light-emitting diodes (LEDs) (Figure S6a). As shown in Figure S6b, the 2.2 μF capacitor is charged by the NCG to 5 V in 300 s under regular walking. Furthermore, by connecting the NCG with three 2.2 μF capacitors in series, the total usable charged voltage is reached at 22.6 V through walking for 10 min (Figure S6c). The stored electric energy is successfully used to drive three commercial green LEDs aligned in a serial circuit (Figure S6d), which demonstrates the potentiality of the developed NCG as energy sources for low-power-consumption electronic devices. Likewise, the NCG is also glued on the elbow of a tight sport suit and then tightly sewn by a piece of cloth (Figure 5c,d). In this way, the NCG is capable of converting energy from the arm movement. In spite of a much smaller stress produced by bending and straightening an arm, visible electric output of 1 V and 10 nA is also obtained, as shown in Figure 5d. Notably, because of the lightweight, ultrathin, and supersoft features of the NCG, it barely exerts any influences on the normal form of the clothing. On the basis of these results, the biocompatible NCG developed in this work might have great potential in wearable device applications, such as energy-harvesting systems inside the shoe, multifunctional wearable nanosensors, and artificial skins.

CONCLUSIONS

In summary, we have realized a fully rollable lead-free NCG with high performance enabled by a piezoelectric active PVDF-niobate-based thin-film nanocomposite and a type of ultraflexible nylon nanofiber-supported AgNW network electrodes. The composition of the NKNS-LT-BZ NPs is found to be located in the PPB region with the coexistence of ferroelectric rhombohedral and tetragonal phases, which significantly enhances the electric output of the NCG. Under periodical agitation at a compressive force of 50 N and 1 Hz, the NCG with an area size of $2 \times 2 \text{ cm}^2$ can generate an optimal V_{OC} and I_{SC} up to 18 V and 2.6 μA , respectively. Notably, the undiminished electric output for the NCG after consecutive rolling cycles indicates its decent rollability. In addition, the potentiality of the NCG in harvesting biomechanical energy from low-frequency human body motions has been further explored. All of the results suggest that the NCG developed in this work is suitable for possible applications, such as fully rollable portable devices, tubular motion nanosensors, and wearable electronic systems, *etc.*

EXPERIMENTAL SECTION

Materials. All of the reagents were used without further purification: analytical-grade metal carbonates and oxides (99%, Sinopharm Co., Ltd.) of Na_2CO_3 , K_2CO_3 , Li_2CO_3 , BaCO_3 , Nb_2O_5 , Sb_2O_5 , Ta_2O_5 , and ZrO_2 ; polymers of PVDF (Sigma-Aldrich), Nylon-6

(PA6, Aladdin), and PDMS (Sylgard 184, Dow Corning, mixed with curing agent in a weight ratio of 10:1); solvents of *N,N*-dimethylformamide (DMF, anhydrous, 99%, Sigma-Aldrich); and formic acid (95%, Sigma-Aldrich).

Fabrication of the NKNS-LT-BZ Perovskite Piezoelectric NPs. Angular NKNS-LT-BZ perovskite NPs were synthesized via a conventional solid-state reaction method according to the nominally compositional formula. Hygroscopic Na_2CO_3 and K_2CO_3 powders were first fully dried at 150 °C to remove the absorbed moisture. The stoichiometric raw powders were thoroughly mixed and ball milled in a nylon jar with zirconia balls at 360 rpm for 12 h using ethanol as the media. The obtained slurries were dried at 80 °C for 12 h and then calcined at 850 °C for 5 h to react and form perovskite crystals. Afterward, the homogeneous compound powders were remilled for 24 h to gain the uniform crystalline NPs.

Fabrication of the PVDF-Niobate-Based Thin-Film Nanocomposite. Perovskite NKNS-LT-BZ NPs with different mass ratios (0–40%) to PVDF powders were first uniformly dispersed in 10 mL of DMF solvent by stirring and ultrasonic dispersing at room temperature for 1 h. Subsequently, PVDF powders were added into the above suspension (10 wt %) and entirely dissolved through vigorous stirring at 65 °C for 3 h. After a treatment in an ultrasonic bath for 1 h again, the uniformly mixed slurries were cast into a film shape in a Petri dish and then degassed and dried in atmosphere at 75 °C. The film thickness could be flexibly adjusted by the amount of casting slurries. The obtained thin-film nanocomposite was annealed in vacuum at 120 °C for 3 h to crystallize the PVDF matrix at last.

Fabrication of the AgNW-Based Electrode and Integration of the PVDF-Niobate-Based NCG. First, the precursor (15 wt %) made by dissolving PA6 particles in the solvent of formic acid was used to prepare the ultrathin nylon nanofiber network via an electrospinning method. Subsequently, the nylon nanofiber network was transferred by a thin polyethylene terephthalate (PET) frame and used as the filtration membrane. The diluted AgNW suspension was vacuum filtrated onto the free-standing nylon nanofiber membrane with the help of a square mask. The as-prepared electrodes were integrated on both major surfaces of the PVDF-niobate-based thin-film nanocomposite with a size of $3 \times 3 \text{ cm}^2$ through a spin-coated adhesive layer of PDMS, and then the NCG was cured at 80 °C for 1 h. The active area of the NCG is about $2 \times 2 \text{ cm}^2$ to prevent electric breakdown at the edges during the poling process. In addition, to minimize the ubiquitous triboelectric effect during the electrical measurement, the NCG was seamlessly vacuum-packed without gaps using two PET thin films to avoid contact-separation motions between the AgNW-based electrode and the mechanical stimulator. Before the electrical measurements, the NCG was poled under a DC field of 20 kV/mm in dry atmosphere at room temperature for 1 h.

Characterization and Measurements. The crystalline structure of the NKNS-LT-BZ NPs and PVDF polymer matrix was determined by the measurements of XRD (D/Max2500 V, Rigaku), Raman (LabRam HR-800), and FT-IR (Nicolet 67) spectra, respectively. The morphology of the thin-film nanocomposite, the AgNW-based electrode, and the NCG was observed using a scanning electron microscope (SU8020). A piezoresponse force microscope (MFP-3D-SA-DV, Asylum Research) was used to investigate the domain switching behavior at nanoscale as well as to measure the d_{33} value of the NKNS-LT-BZ NPs. The Pt-coated tip (Asyelec-01, Asylum Research) with a spring constant of 2 N/m was used for the PFM measurements. The sheet resistance of the AgNW-based electrode was measured using a resistivity measurement system (RTS-9) with a four-point probe configuration to eliminate the contact resistance. The electric output of the NCG was measured by low-noise voltage preamplifiers (Keithley 6514 System Electrometer and Stanford Research SR570).

ASSOCIATED CONTENT

Supporting Information

The Supporting Information is available free of charge on the ACS Publications website at DOI: 10.1021/acsnano.8b01534.

Percentage sheet resistance change, FT-IR spectra, OP-PFM phase images, top-view SEM micrographs, schematic circuit diagram, composition design, quasi-static d_{33} and electromechanical coupling coefficient k_p , and the force applying setup (PDF)

AUTHOR INFORMATION

Corresponding Authors

*E-mail: chenaihua@buaa.edu.cn.

*E-mail: zhuguang@binn.cas.cn.

*E-mail: wangzhonglin@binn.cas.cn.

ORCID

Aihua Chen: 0000-0002-9609-988X

Guang Zhu: 0000-0003-2350-0369

Zhong Lin Wang: 0000-0002-5530-0380

Author Contributions

C.Z. and Y.J.F. contributed equally to this work.

Notes

The authors declare no competing financial interest.

ACKNOWLEDGMENTS

The authors gratefully acknowledge the financial support from the National Natural Science Foundation of China (Grants 51472018, 51272010, 21673014, and 51572030), National Key R&D Project from Ministry of Science and Technology, China (Grants 2016YFA0202701 and 2016YFA0202703), Beijing Natural Science Foundation (Grant 2162047), Beijing Nova Program (XX2013009), Research Fund for the Doctoral Program of Higher Education (20121102120001), and Fundamental Research Funds for the Central Universities (YWF-16-BJ-Y-75).

REFERENCES

- (1) Beggs, C. *Energy: Management, Supply and Conservation*; Elsevier: Oxford, 2002.
- (2) Hwang, G. T.; Byun, M.; Jeong, C. K.; Lee, K. J. Flexible Piezoelectric Thin-Film Energy Harvesters and Nanosensors for Biomedical Applications. *Adv. Healthcare Mater.* **2015**, *4*, 646–658.
- (3) Hu, Y. F.; Wang, Z. L. Recent Progress in Piezoelectric Nanogenerators as a Sustainable Power Source in Self-Powered Systems and Active Sensors. *Nano Energy* **2015**, *14*, 3–14.
- (4) Lee, S. H.; Jeong, C. K.; Hwang, G. T.; Lee, K. J. Self-Powered Flexible Inorganic Electronic System. *Nano Energy* **2015**, *14*, 111–125.
- (5) Fan, F. R.; Tang, W.; Wang, Z. L. Flexible Nanogenerators for Energy Harvesting and Self-Powered Electronics. *Adv. Mater.* **2016**, *28*, 4283–4305.
- (6) Wang, Z. L.; Song, J. H. Piezoelectric Nanogenerators Based on Zinc Oxide Nanowire Arrays. *Science* **2006**, *312*, 242–246.
- (7) Koka, A.; Zhou, Z.; Sodano, H. A. Vertically Aligned BaTiO_3 Nanowire Arrays for Energy Harvesting. *Energy Environ. Sci.* **2014**, *7*, 288–296.
- (8) Mao, Y. C.; Zhao, P.; McConohy, G.; Yang, H.; Tong, Y. X.; Wang, X. D. Sponge-Like Piezoelectric Polymer Films for Scalable and Integratable Nanogenerators and Self-Powered Electronic Systems. *Adv. Energy Mater.* **2014**, *4*, 1301624.
- (9) Hansen, B. J.; Liu, Y.; Yang, R. S.; Wang, Z. L. Hybrid Nanogenerator for Concurrently Harvesting Biomechanical and Biochemical Energy. *ACS Nano* **2010**, *4*, 3647–3652.
- (10) Sun, C. L.; Shi, J.; Bayerl, D. J.; Wang, X. D. PVDF Microbelts for Harvesting Energy from Respiration. *Energy Environ. Sci.* **2011**, *4*, 4508–4512.
- (11) Wang, X. D.; Song, J. H.; Liu, J.; Wang, Z. L. Direct Current Nanogenerator Driven by Ultrasonic Wave. *Science* **2007**, *316*, 102–105.

- (12) Cha, S. N.; Seo, J. S.; Kim, S. M.; Kim, H. J.; Park, Y. J.; Kim, S. W.; Kim, J. M. Sound-Driven Piezoelectric Nanowire-Based Nanogenerators. *Adv. Mater.* **2010**, *22*, 4726–4730.
- (13) Lee, J. H.; Lee, K. Y.; Kumar, B.; Tien, N. T.; Lee, N. E.; Kim, S. W. Highly Sensitive Stretchable Transparent Piezoelectric Nanogenerators. *Energy Environ. Sci.* **2013**, *6*, 169–175.
- (14) Park, K. I.; Lee, M.; Liu, Y.; Moon, S.; Hwang, G. T.; Zhu, G.; Kim, J. E.; Kim, S. O.; Kim, D. K.; Wang, Z. L.; Lee, K. J. Flexible Nanocomposite Generator Made of BaTiO₃ Nanoparticles and Graphitic Carbons. *Adv. Mater.* **2012**, *24*, 2999–3004.
- (15) Jeong, C. K.; Lee, J.; Han, S.; Ryu, J.; Hwang, G. T.; Park, D. Y.; Park, J. H.; Lee, S. S.; Byun, M.; Ko, S. H.; Lee, K. J. A Hyper-Stretchable Elastic-Composite Energy Harvester. *Adv. Mater.* **2015**, *27*, 2866–2875.
- (16) Zhu, G.; Wang, A. C.; Liu, Y.; Zhou, Y. S.; Wang, Z. L. Functional Electrical Stimulation by Nanogenerator with 58 V Output Voltage. *Nano Lett.* **2012**, *12*, 3086–3090.
- (17) Hu, Y. F.; Zhang, Y.; Xu, C.; Lin, L.; Snyder, R. L.; Wang, Z. L. Self-Powered System with Wireless Data Transmission. *Nano Lett.* **2011**, *11*, 2572–2577.
- (18) Wang, C. H.; Liao, W. S.; Lin, Z. H.; Ku, N. J.; Li, Y. C.; Chen, Y. C.; Wang, Z. L.; Liu, C. P. Optimization of the Output Efficiency of GaN Nanowire Piezoelectric Nanogenerators by Tuning the Free Carrier Concentration. *Adv. Energy Mater.* **2014**, *4*, 1400392.
- (19) Wu, W. Z.; Wang, L.; Li, Y. L.; Zhang, F.; Lin, L.; Niu, S. M.; Chenet, D.; Zhang, X.; Hao, Y. F.; Heinz, T. F.; Hone, J.; Wang, Z. L. Piezoelectricity of Single-Atomic-Layer MoS₂ for Energy Conversion and Piezotronics. *Nature* **2014**, *514*, 470–474.
- (20) Qi, Y.; Kim, J.; Nguyen, T. D.; Lisko, B.; Purohit, P. K.; McAlpine, M. C. Enhanced Piezoelectricity and Stretchability in Energy Harvesting Devices Fabricated from Buckled PZT Ribbons. *Nano Lett.* **2011**, *11*, 1331–1336.
- (21) Park, K. I.; Son, J. H.; Hwang, G. T.; Jeong, C. K.; Ryu, J.; Koo, M.; Choi, I.; Lee, S. H.; Byun, M.; Wang, Z. L.; Lee, K. J. Highly-Efficient, Flexible Piezoelectric PZT Thin Film Nanogenerator on Plastic Substrates. *Adv. Mater.* **2014**, *26*, 2514–2520.
- (22) Hwang, G. T.; Park, H.; Lee, J. H.; Oh, S.; Park, K. I.; Byun, M.; Park, H.; Ahn, G.; Jeong, C. K.; No, K.; Kwon, H. S.; Lee, S. G.; Joung, B.; Lee, K. J. Self-Powered Cardiac Pacemaker Enabled by Flexible Single Crystalline PMN-PT Piezoelectric Energy Harvester. *Adv. Mater.* **2014**, *26*, 4880–4887.
- (23) Park, K. I.; Xu, S.; Liu, Y.; Hwang, G. T.; Kang, S. L.; Wang, Z. L.; Lee, K. J. Piezoelectric BaTiO₃ Thin Film Nanogenerator on Plastic Substrates. *Nano Lett.* **2010**, *10*, 4939–4943.
- (24) Kim, Y. J.; Dang, T. V.; Choi, H. J.; Park, B. J.; Eom, J. H.; Song, H. A.; Seol, D.; Kim, Y.; Shin, S. H.; Nah, H.; Yoon, S. G. Piezoelectric Properties of CH₃NH₃PbI₃ Perovskite Thin Films and Their Applications in Piezoelectric Generators. *J. Mater. Chem. A* **2016**, *4*, 756–763.
- (25) Jung, J. H.; Lee, M.; Hong, J. I.; Ding, Y.; Chen, C. Y.; Chou, L. J.; Wang, Z. L. Lead-Free NaNbO₃ Nanowires for a High Output Piezoelectric Nanogenerator. *ACS Nano* **2011**, *5*, 10041–10046.
- (26) Park, K. I.; Jeong, C. K.; Ryu, J.; Hwang, G. T.; Lee, K. J. Flexible and Large-Area Nanocomposite Generators Based on Lead Zirconate Titanate Particles and Carbon Nanotubes. *Adv. Energy Mater.* **2013**, *3*, 1539–1544.
- (27) Jeong, C. K.; Park, K. I.; Ryu, J.; Hwang, G. T.; Lee, K. J. Large-Area and Flexible Lead-Free Nanocomposite Generator Using Alkaline Niobate Particles and Metal Nanorod Filler. *Adv. Funct. Mater.* **2014**, *24*, 2620–2629.
- (28) Sun, H.; Tian, H.; Yang, Y.; Xie, D.; Zhang, Y. C.; Liu, X.; Ma, S.; Zhao, H. M.; Ren, T. L. A Novel Flexible Nanogenerator Made of ZnO Nanoparticles and Multiwall Carbon Nanotube. *Nanoscale* **2013**, *5*, 6117–6123.
- (29) Zhou, Z.; Tang, H. X.; Sodano, H. A. Scalable Synthesis of Morphotropic Phase Boundary Lead Zirconium Titanate Nanowire for Energy Harvesting. *Adv. Mater.* **2014**, *26*, 7547–7554.
- (30) Baek, C.; Yun, J. H.; Wang, J. E.; Jeong, C. K.; Lee, K. J.; Park, K. I.; Kim, D. K. A Flexible Energy Harvester Based on a Lead-Free and Piezoelectric BCTZ Nanoparticle-Polymer Composite. *Nanoscale* **2016**, *8*, 17632–17638.
- (31) Ding, R.; Liu, H.; Zhang, X. L.; Xiao, J. X.; Kishor, R.; Sun, H. X.; Zhu, B. W.; Chen, G.; Gao, F.; Feng, X. H.; Chen, J. S.; Chen, X. D.; Sun, X. W.; Zheng, Y. J. Flexible Piezoelectric Nanocomposite Generators Based on Formamidinium Lead Halide Perovskite Nanoparticles. *Adv. Funct. Mater.* **2016**, *26*, 7708–7716.
- (32) Park, K. I.; Jeong, C. K.; Kim, N. K.; Lee, K. J. Stretchable Piezoelectric Nanocomposite Generator. *Nano Convergence* **2016**, *3*, 12.
- (33) Lee, J. H.; Lee, K. Y.; Gupta, M. K.; Kim, T. Y.; Lee, D. Y.; Oh, J.; Ryu, C.; Yoo, W. J.; Kang, C. Y.; Yoon, S. J.; Yoo, J. B.; Kim, S. W. Highly Stretchable Piezoelectric-Pyroelectric Hybrid Nanogenerator. *Adv. Mater.* **2014**, *26*, 765–769.
- (34) Shin, S. H.; Kim, Y. H.; Lee, M. H.; Jung, J. Y.; Nah, J. Hemispherically Aggregated BaTiO₃ Nanoparticle Composite Thin Film for High-Performance Flexible Piezoelectric Nanogenerator. *ACS Nano* **2014**, *8*, 2766–2773.
- (35) Siddiqui, S.; Kim, D. I.; Duy, L. T.; Nguyen, M. T.; Muhammad, S.; Yoon, W. S.; Lee, N. E. High-Performance Flexible Lead-Free Nanocomposite Piezoelectric Nanogenerator for Biomechanical Energy Harvesting and Storage. *Nano Energy* **2015**, *15*, 177–185.
- (36) Wang, K.; Yao, F. Z.; Jo, W.; Gobeljic, D.; Shvartsman, V. V.; Lupascu, D. C.; Li, J. F.; Rödel, J. Temperature-Insensitive (K,Na)NbO₃-Based Lead-Free Piezoactuator Ceramics. *Adv. Funct. Mater.* **2013**, *23*, 4079–4086.
- (37) Wang, X. P.; Zheng, T.; Wu, J. G.; Xiao, D. Q.; Zhu, J. G.; Wang, H.; Wang, X. J.; Lou, X. J.; Gu, Y. L. Characteristics of Giant Piezoelectricity around the Rhombohedral-Tetragonal Phase Boundary in (K, Na)NbO₃-Based Ceramics with Different Additives. *J. Mater. Chem. A* **2015**, *3*, 15951.
- (38) Wu, H.; Kong, D. S.; Ruan, Z. C.; Hsu, P. C.; Wang, S.; Yu, Z. F.; Carney, T. J.; Hu, L. B.; Fan, S. H.; Cui, Y. A Transparent Electrode Based on a Metal Nanotrough Network. *Nat. Nanotechnol.* **2013**, *8*, 421–425.
- (39) Lee, P.; Lee, J.; Lee, H.; Yeo, J.; Hong, S.; Nam, K. H.; Lee, D.; Lee, S. S.; Ko, S. H. Highly Stretchable and Highly Conductive Metal Electrode by Very Long Metal Nanowire Percolation Network. *Adv. Mater.* **2012**, *24*, 3326–3332.
- (40) Zhao, Y. B.; Chen, A. H.; Liang, S. Shape-Controlled Synthesis of Silver Nanocrystals via γ -Irradiation in the Presence of Poly(vinyl pyrrolidone). *J. Cryst. Growth* **2013**, *372*, 116.
- (41) Saip, J. A. B.; Moor, E. R.; Cabrera, A. L. Raman Study of Phase Transitions in KNbO₃. *Solid State Commun.* **2005**, *135*, 367–372.
- (42) Ross, S. D. The Vibrational Spectra of Lithium Niobate, Barium Sodium Niobate and Barium Sodium Tantalate. *J. Phys. C: Solid State Phys.* **1970**, *3*, 1785.
- (43) Klein, N.; Hollenstein, E.; Damjanovic, D.; Trodahl, H. J.; Setter, N.; Kuball, M. A Study of the Phase Diagram of (K,Na,Li)-NbO₃ Determined by Dielectric and Piezoelectric Measurements, and Raman Spectroscopy. *J. Appl. Phys.* **2007**, *102*, 014112.
- (44) Bhavanasri, V.; Kumar, V.; Parida, K.; Wang, J. X.; Lee, P. S. Enhanced Piezoelectric Energy Harvesting Performance of Flexible PVDF-TrFE Bilayer Films with Graphene Oxide. *ACS Appl. Mater. Interfaces* **2016**, *8*, 521–529.
- (45) Sinha, T. K.; Ghosh, S. K.; Maiti, R.; Jana, S.; Adhikari, B.; Mandal, D.; Ray, S. K. Graphene-Silver-Induced Self-Polarized PVDF-Based Flexible Plasmonic Nanogenerator Toward the Realization for New Class of Self Powered Optical Sensor. *ACS Appl. Mater. Interfaces* **2016**, *8*, 14986–14993.
- (46) Anthoniappen, J.; Chang, W. S.; Soh, A. K.; Tu, C. S.; Vashan, P.; Lim, F. S. Electric Field Induced Nanoscale Polarization Switching and Piezoresponse in S_m and M_n Co-Doped BiFeO₃ Multiferroic Ceramics by Using Piezoresponse Force Microscopy. *Acta Mater.* **2017**, *132*, 174–181.
- (47) Bhimireddi, R.; Ponraj, B.; Varma, K. B. R. Structural, Optical, and Piezoelectric Response of Lead-Free Ba_{0.95}Mg_{0.05}Zr_{0.1}Ti_{0.9}O₃ Nanocrystalline Powder. *J. Am. Ceram. Soc.* **2016**, *99*, 896–904.

(48) Ghasemian, M. B.; Lin, Q. R.; Adabifiroozjaei, E.; Wang, F. F.; Chu, D. W.; Wang, D. Y. Morphology Control and Large Piezoresponse of Hydrothermally Synthesized Lead-Free Piezoelectric $(\text{Bi}_{0.5}\text{Na}_{0.5})\text{TiO}_3$ Nanofibres. *RSC Adv.* **2017**, *7*, 15020–15026.

(49) Lee, D. Y.; Kim, H.; Li, H. M.; Jang, A. R.; Lim, Y. D.; Cha, S. N.; Park, Y. J.; Kang, D. J.; Yoo, W. J. Hybrid Energy Harvester Based on Nanopillar Solar Cells and PVDF Nanogenerator. *Nanotechnology* **2013**, *24*, 175402.

(50) Dhakras, D.; Borkar, V.; Ogale, S.; Jog, J. Enhanced Piezoresponse of Electrospun PVDF Mats with a Touch of Nickel Chloride Hexahydrate Salt. *Nanoscale* **2012**, *4*, 752–756.

(51) Cha, S.; Kim, S. M.; Kim, H.; Ku, J.; Sohn, J. L.; Park, Y. J.; Song, B. G.; Jung, M. H.; Lee, E. K.; Choi, B. L.; Park, J. J.; Wang, Z. L.; Kim, J. M.; Kim, K. Porous PVDF as Effective Sonic Wave Driven Nanogenerators. *Nano Lett.* **2011**, *11*, 5142–5147.

(52) Lee, K. Y.; Kim, D.; Lee, J. H.; Kim, T. Y.; Gupta, M. K.; Kim, S. W. Unidirectional High-Power Generation *via* Stress-Induced Dipole Alignment from ZnSnO_3 Nanocubes/Polymer Hybrid Piezoelectric Nanogenerator. *Adv. Funct. Mater.* **2014**, *24*, 37–43.

(53) Choi, D.; Choi, M. Y.; Choi, W. M.; Shin, H. J.; Park, H. K.; Seo, J. S.; Park, J.; Yoon, S. M.; Chae, S. J.; Lee, Y. H.; Kim, S. W.; Choi, J. Y.; Lee, S. Y.; Kim, J. M. Fully Rollable Transparent Nanogenerators Based on Graphene Electrodes. *Adv. Mater.* **2010**, *22*, 2187–2192.

(54) Liang, Q. J.; Zhang, Q.; Yan, X. Q.; Liao, X. Q.; Han, L. H.; Yi, F.; Ma, M. Y.; Zhang, Y. Recyclable and Green Triboelectric Nanogenerator. *Adv. Mater.* **2017**, *29*, 1604961.

(55) Fan, Y. J.; Meng, X. S.; Li, H. Y.; Kuang, S. Y.; Zhang, L.; Wu, Y.; Wang, Z. L.; Zhu, G. Stretchable Porous Carbon Nanotube-Elastomer Hybrid Nanocomposite for Harvesting Mechanical Energy. *Adv. Mater.* **2017**, *29*, 1603115.